Evidence for the earliest hominin use of wooden handheld tools found at Marathousa 1 (Greece)

Article

Supplemental Material

SUPPLEMENTARY INFORMATION: Evidence for the earliest hominin use of wooden handheld tools found at Marathousa 1 (Greece)

This paper is published in Proceedings of the National Academy of Sciences: https://doi.org/10.1073/pnas.2515479123

Please cite this paper as: A. Milks, M. Ntinou, S. Koutalis, D. Michailidis, G.E. Konidaris, D. Giusti, N. Thompson, G. Tsartsidou, E. Panagopoulou, V. Tourloukis, P. Karkanas, & K. Harvati, Evidence for the earliest hominin use of wooden handheld tools found at Marathousa 1 (Greece), Proc. Natl. Acad. Sci. U.S.A. 123 (6) e2515479123, https://doi.org/10.1073/pnas.2515479123 (2026).

Authors

Annemieke Milks[*,a], Maria Ntinou[b], Stylianos Koutalis[c], Dimitrios Michailidis[d], George E. Konidaris[c,e], Domenico Giusti[c,f], Nicholas Thompson[c], Georgia Tsartsidou[g,d], Eleni Panagopoulou[g], Vangelis Tourloukis [c,h], Panagiotis Karkanas[d], Katerina Harvati [*,c,f,i,j]

a. University of Reading, Department of Archaeology
b. Aristotle University of Thessaloniki, School of History and Archaeology
c. Paleoanthropology, Institute for Archaeological Sciences, Department of Geosciences, Eberhard Karls University of Tübingen
d. M.H. Wiener Laboratory for Archaeological Science, American School of Classical Studies at Athens
e. Aristotle University of Thessaloniki, School of Geology
f. Senckenberg Centre for Human Evolution and Palaeoenvironment, Department of Geosciences, Eberhard Karls University of Tübingen
g. Ephorate of Paleoanthropology and Speleology, Hellenic Ministry of Culture
h. University of Ioannina, School of Archaeology
i. DFG Centre for Advanced Studies 'Words, Bones, Genes, Tools: Tracking linguistic, cultural and biological trajectories of the human past', Eberhard Karls University of Tübingen
j. HUMAN ORIGINS – Cluster of Excellence for Integrative Human Origins Studies (EXC 3101), Eberhard Karls University of Tübingen, Tübingen, Germany

*Co-corresponding authors
Annemieke Milks, email: a.g.milks@reading.ac.uk
Katerina Harvati, email: katerina.harvati@ifu.uni-tuebingen.de

1. Supplementary tables

Table S1. Number of plotted wood specimens excavated in MAR-1 (2015-2019).

Stratigraphic Unit	Number of wood remains plotted
AREA A	
UA3b	1
UA3c	66
UA4	55
AREA B	
UB3c	2
UB4a	1
UB4c	18
UB5b/UB5c	1
TOTAL	**144**

Table S2: Wood specimens showing anthropogenic (Categories 1 and 2), possible anthropogenic (Categories 3 and 4) and carnivore modifications. The specimens presented in detail in the text are shown in bold. Category definitions after Leder et al. (1), see Table S3.

Area	Year	Trench	ID	Unit / Spit	Z	Category	Species
A	**2015**	**940/673**	**39**	**UA3c, Spit 3**	**349,15**	**1**	***Alnus* sp.**
A	**2018**	**935/671**	**13**	**UA4, Spit 1**	**349,48**	**2**	***Salix* sp. / *Populus* sp.**
A	2016	937/673	33	UA4, Spit 2	349,19	3	*Salix*
A	2015	941/677	47	UA3c, Spit 4	349,26	4	*Salix*
A	2015	941/677	46	UA3c, Spit 4	349,88	4	*angiosperm*
B	2015	932/599	23	UB4c, Spit 4	350,55	4	*Salix sp. / Populus* sp.
A	2015	940/973	42	UA4, Spit 1	349,07	4	*Salix sp./Populus* sp.
A	**2016**	**942/677**	**59**	**UA4, Spit 2**	**349,2**	**Non-anthropogenic**	***Alnus* sp.**

Table S3: Framework for wood artefact categories, after Leder et al. (1).

Category 1	bear definitive working traces. Different tool mark types are present on a single item and often more than once per type.
Category 2	bear multiple probable working traces, sometimes less clear due to preservation, which occur in various combinations.
Category 3	bear possible working traces in combinations of at least two different tool mark types.
Category 4	lack diagnostic tool marks often due to an advanced taphonomic deterioration of surfaces

Table S4. Distances and angles taken from the cross-sectional profiles measured for each of the gouges of specimen 942/677-59, interpreted to represent claw marks. Measurements according to Bello et al. (2) and Maté González et al. (3). Abbreviations: **WIS**, width of the incision at the surface; **WIM**, width of the incision at then mean; **WIB**, width of the incision at its bottom; **OA**, opening angle of the incision; **D**, depth of the incision; **RDC**, right depth of the incision; **LDC**, left depth of the incision.

Marks	**1**			**2**			**3**			
L (cm)	17.8			15.3			20.7			
Sections	**1A**	**1B**	**1C**	**2A**	**2B**	**2C**	**3A**	**3B**	**3C**	**3D**
WIS (mm)	4,57	5,91	3,51	5,01	3,5	5,08	9,88	10,03	7,07	9,5
WIM (mm)	2,26	2,43	1,55	2,79	1,76	2,81	4,91	5,25	3,59	5,15
WIB (mm)	0,96	1,23	0,89	1,37	0,82	1,26	1,49	2,03	1,95	1,91
OA (°)	76,7	92,6	106,7	110,1	120	104,2	120,45	102,86	90,75	104,32
D (mm)	2,18	2,14	0,92	1,54	0,84	1,71	1,59	2,79	2,9	3,04
RDC (mm)	3,6	3,78	2,39	3,69	2,21	3,1	3,06	4,49	4,03	5,73
LDC (mm)	2,75	3,55	1,59	2,28	1,74	3,09	7,45	7,06	5,23	5,53

2. Supplementary Figures

Figure S1: MAR-1 profile, showing the locations of the excavation areas A and B and the stratigraphic profile exposed on the section, before the initiation of excavation in 2013.

Figure S2: Overview of Area A, end of excavation season 2015 (center), showing the *P. antiquus* skeletal remains *in situ*, excavated in association with large and smaller wood remains (panels **a-e**). Panels: **a)** excavation photograph of part of Specimen 942/677-59; **b,c,e)** photographs showing wood remains excavated among the elephant bones; **d)** excavation photograph of Specimen 935/671-13. Panels a-e are shown close to their approximate positions in the trench. Orientation of the trench as in Figure 1.

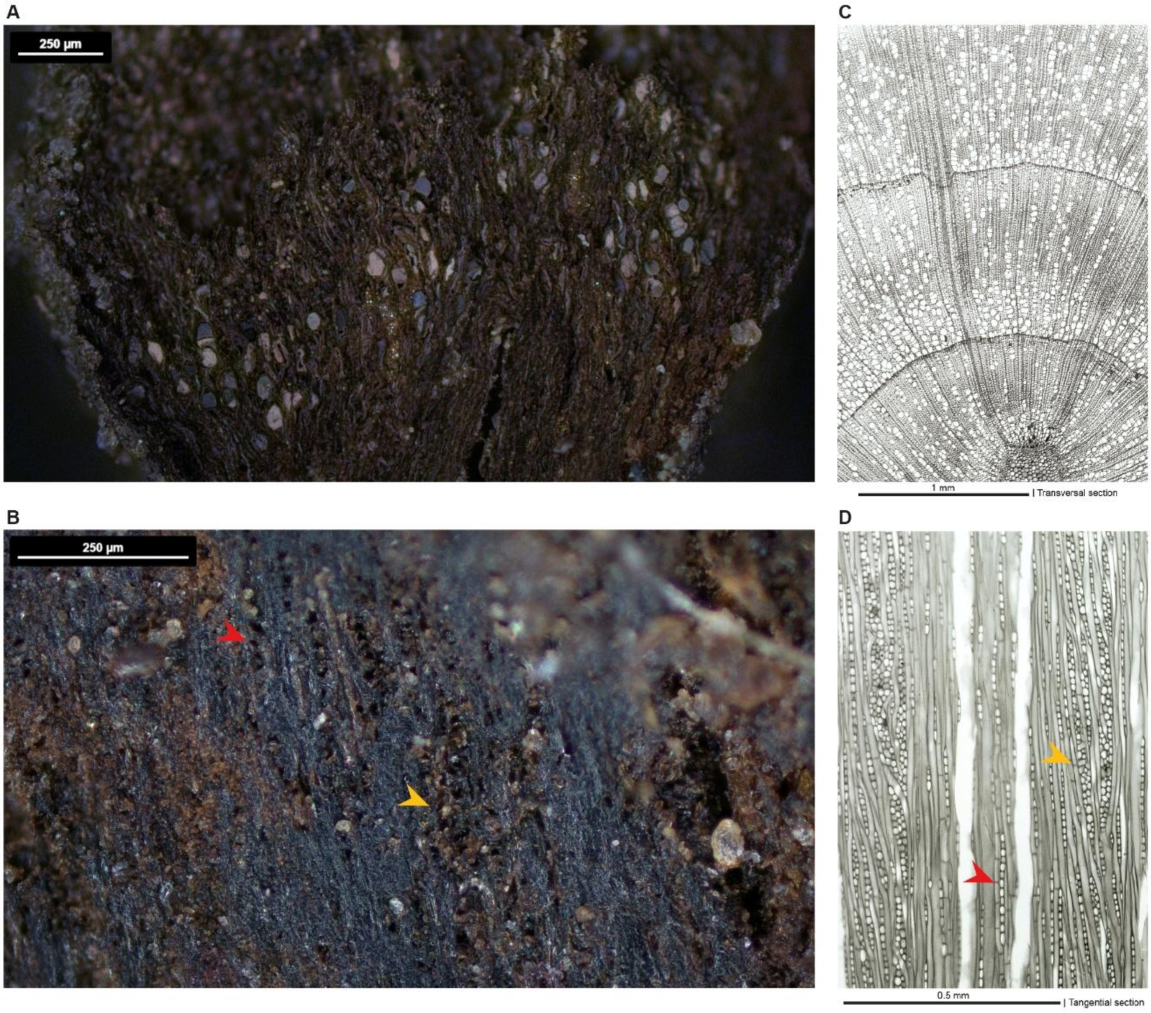

Figure S3: **A)** Transversal section of the wood of 940/673-39, *Alnus* sp. **B)** Tangential section of the wood of specimen 59, *Alnus* sp. **C**) Transversal section of *Alnus glutinosa* Gaertn. (ALGL10). **D**) Tangential section of *Alnus glutinosa* Gaertn. (ALGL24). Note the highly compressed structure in A. Uniseriate (red arrows) and aggregate rays (yellow arrows) can be seen in B and D. Micrographs of specimens 39 and 59 (A, B) M. Ntinou. Comparative material (**C**) from Schoch et al (4). Reproduced with permission from W. Schoch, who retains the copyright for these images.

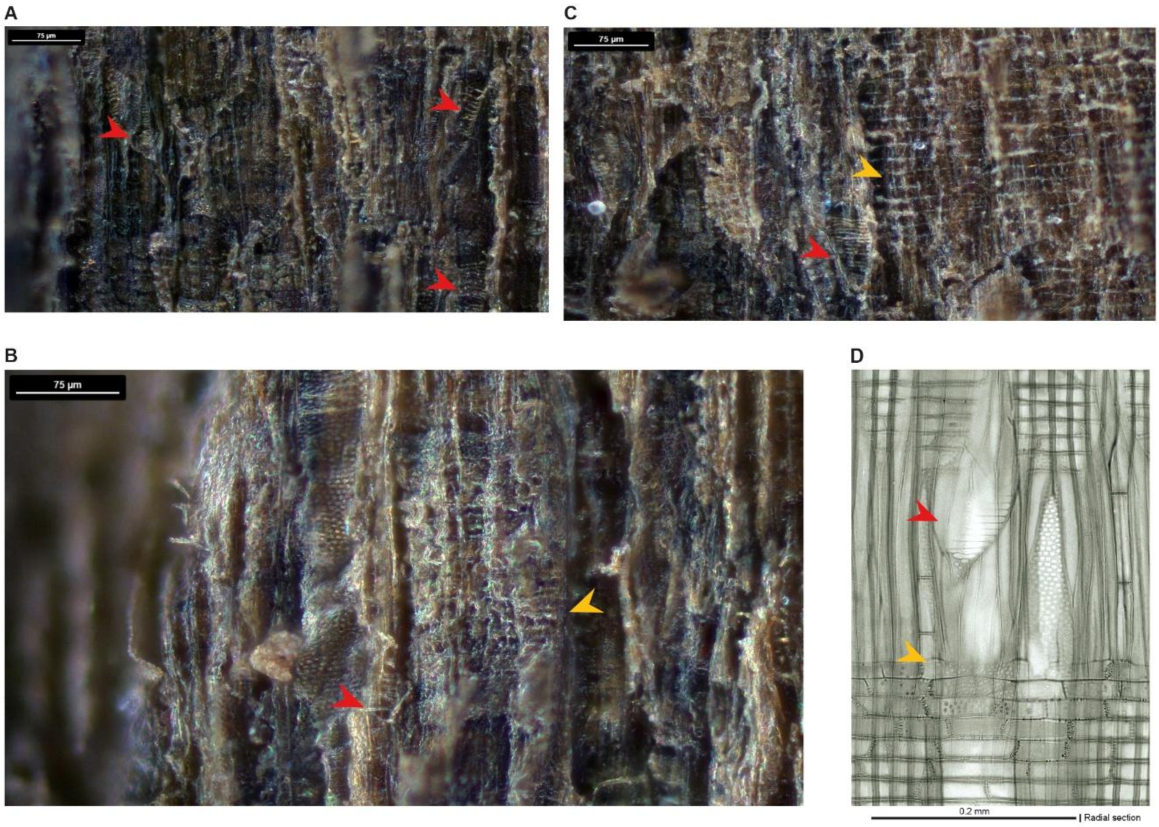

Figure S4: **A)** Radial section of the wood of 940/673-39, *Alnus* sp. **B)** Radial section of the wood of specimen 39, *Alnus* sp. **C)** Radial section of the wood of specimen 59, *Alnus* sp. **D**) Radial section of *Alnus glutinosa* Gaertn. (ALGL20). Note scalariform perforation plates (red arrows) and homogeneous rays (yellow arrows). Micrographs of specimens 39 and 59 (**A, B, C**) M. Ntinou. Comparative material (**D**) from Schoch et al (4). Reproduced with permission from W. Schoch, who retains the copyright for these images.

Figure S5: The functional end of 940/673-39, View 3. The pink highlighted area shows where the wood fibres show micro-damage, likely from use (see also Figure 2c in main manuscript, and Figures S4 and S5).

Figure S6: The functional end of 940/673-39. **Left**: Rounding and micro-splintering interpreted as usewear, on Fragment 4, View 1, 81 cm. **Right**: Micro-splintering focused on Fragment 4, View 3. Note where the micro-splintering ends, and the surface becomes regular. Fragment 4, View 3, 81 cm. Leica microscope images.

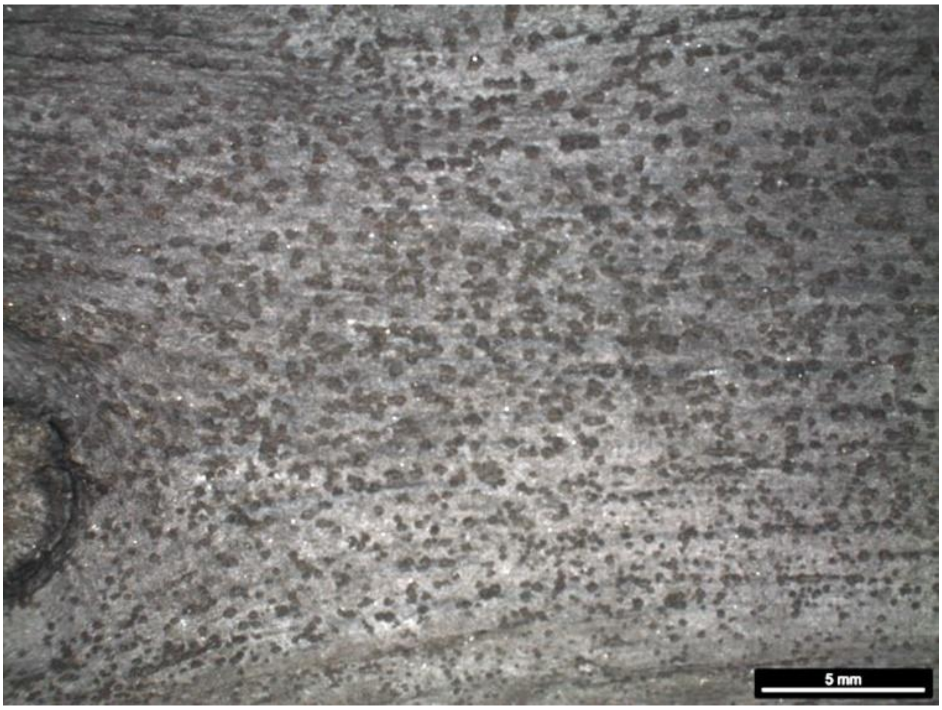

Figure S7: Pitting on the surface of 940/673-39. Fragment 2, View 1. Leica microscope image.

Figure S8: 940/673 ID 39. Fragment 1, View 1, 8.8 – 10 cm. Recent damage, excavation or post-excavation phase. Leica microscope image.

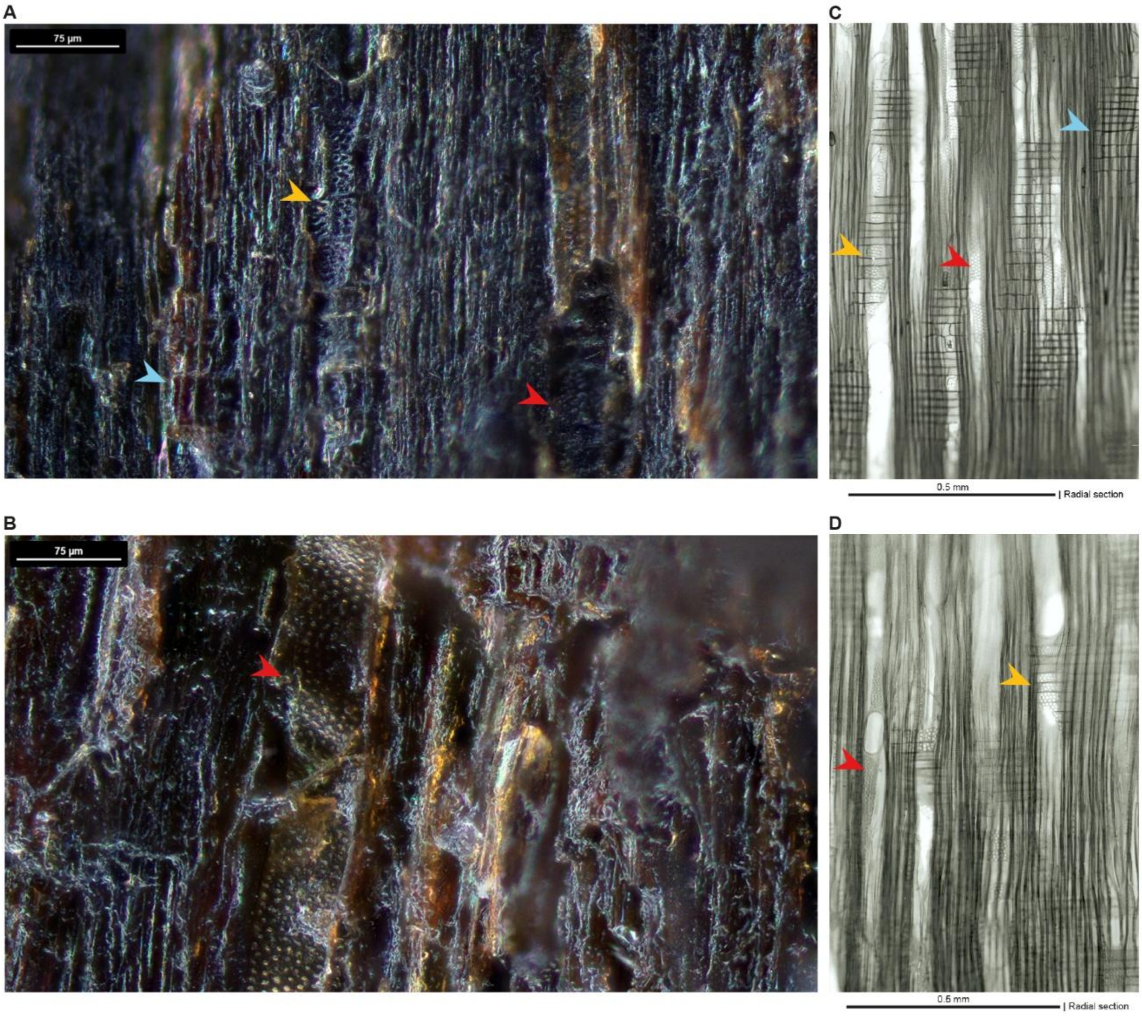

Figure S9: **A** and **B)** Radial sections of the wood of 935/671-13, *Salix* sp./*Populus* sp. **C**) Radial section of *Salix cinerea* L. (SACI17). **D**) Radial section of *Populus alba* L. (PPAL19). Note large intervessel pits (red arrows), large, simple ray-vessel pits (yellow arrows), rays with rows of upright marginal cells characterizing the genus *Salix* (blue arrows) and possibly present in the wood of specimen 13. Micrographs of specimen 13 (**A, B**) M. Ntinou. Comparative material **(C, D)** from Schoch et al (4). Reproduced with permission from W. Schoch, who retains the copyright for these images.

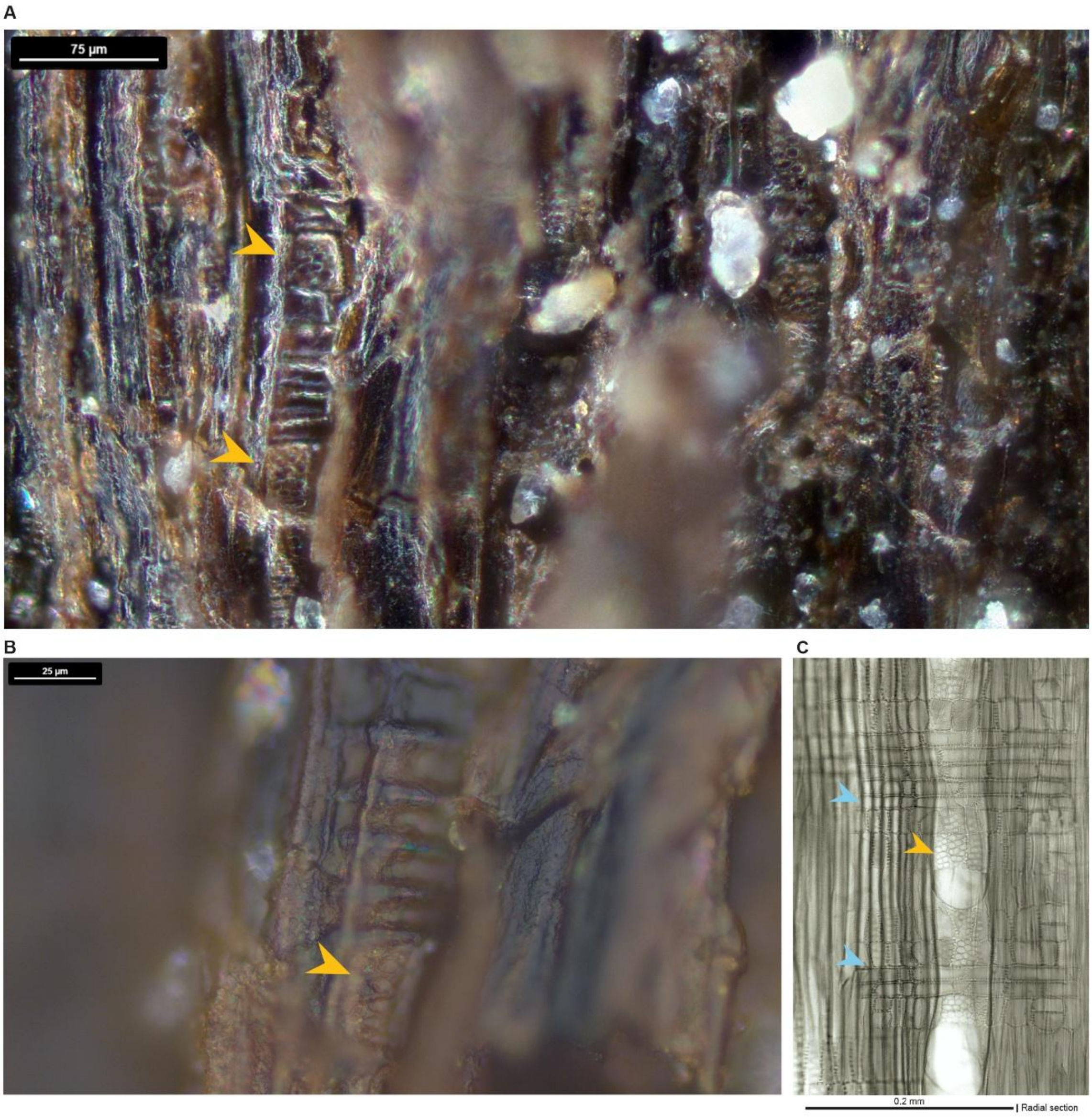

Figure S10: **A** and **B)** Radial sections of the wood of 935/671-13, *Salix* sp./*Populus* sp. **C)** Radial section of *Salix incana* (SAIN18). Note large, simple ray-vessel pits (yellow arrows). The heterogeneous rays of **C** (blue arrows) can be compared with Figure S10.A of specimen 13. Micrographs of specimen 13 (**A, B**) M. Ntinou. Comparative material (**C**) from Schoch et al (4). Reproduced with permission from W. Schoch, who retains the copyright for these images.

Figure S11: 935/671-13. Close-up of worked area (see also Figure S12, Left).

Figure S12: Possible tool marks on 935/671-13. **Left:** Tool facet with side features, signature, and stop mark, at 8x magnification. White arrow indicates the direction of the tool facet. View 1, 0.5 to 1 cm. Leica microscope image. **Right:** Group of parallel striations on View 1 running obliquely to the grain, area of striations highlighted in white circle. Leica microscope image.

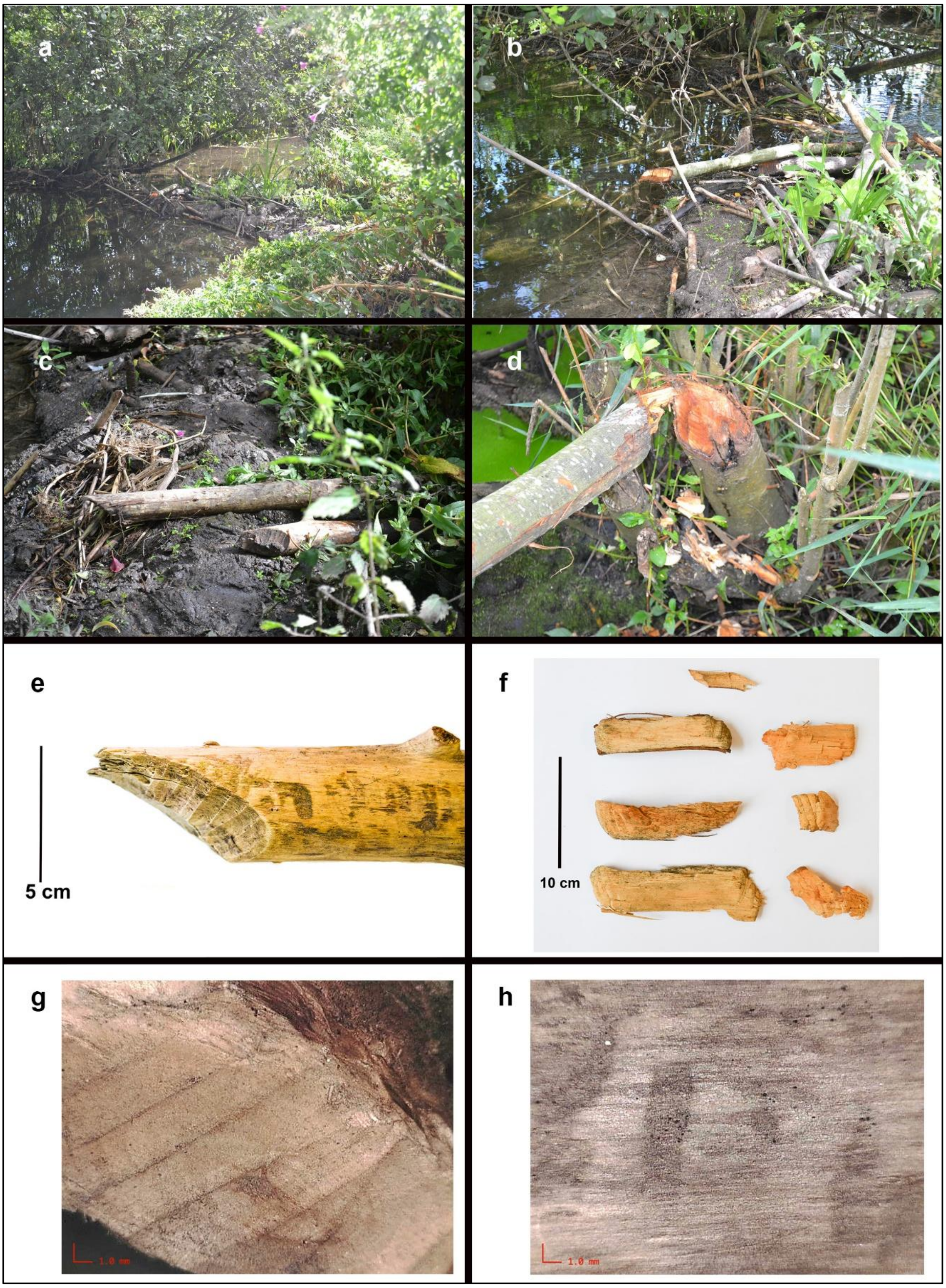

Figure S13. Beaver activity and beaver-gnawed wood from the beaver conservation area of Ham Fen, Kent, U.K. **a)** beaver dam. **b** and **c)** chewed branches forming part of the beaver dam. **d)** a willow tree and wood chips, felled by beaver. **e)** beaver-gnawed branch end collected from the dam displaying facets along the cut face, and shallow gnawing as dark patches running parallel to growth along the branch shaft **f)** various wood chips collected from around the felled tree **g)** microscopic image (20x) of a beaver-gnawed branch, displaying characteristic facets running obliquely to the growth **h)** microscopic image (20x) of shallow grooves running parallel to the branch growth. Images by A. Milks.

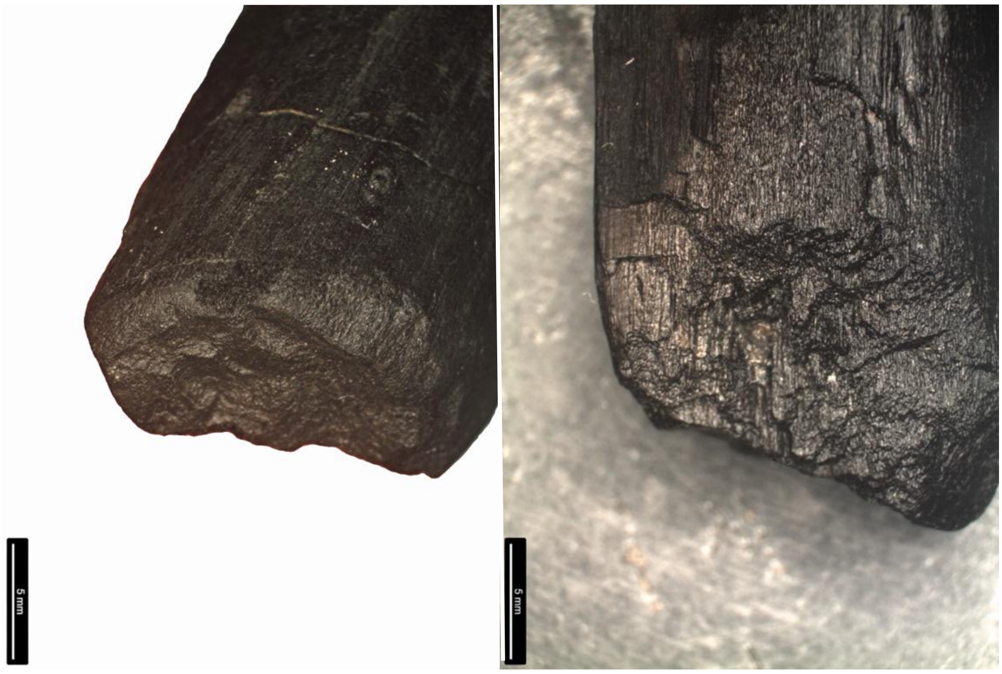

Figure S14: Left: Area of rounding at ‘base’ of tool 935/671-13. View 1. Right: Series of stepped splinter negatives located at ‘base’ of tool 935/671-13, View 3. Leica microscope images.

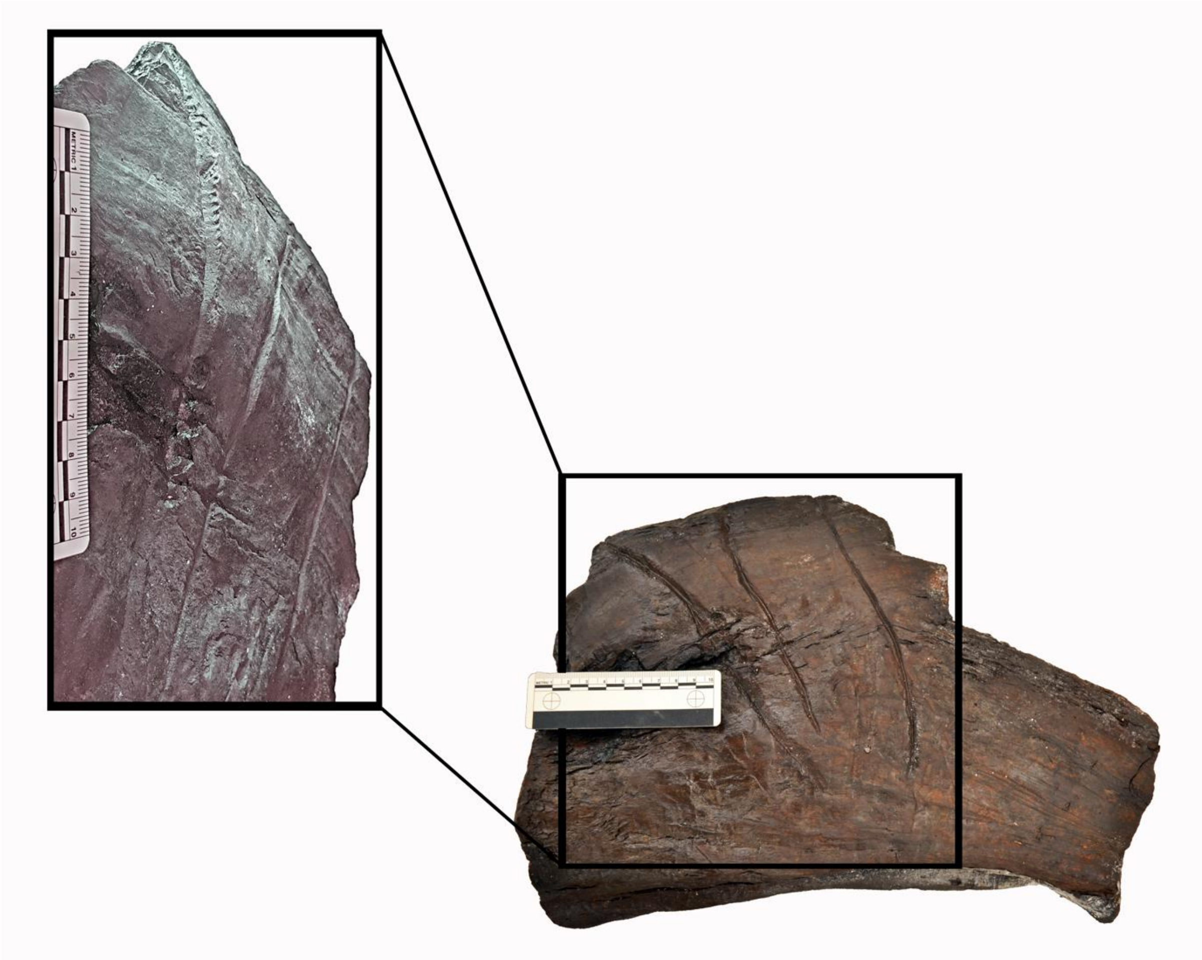

Figure S15: Overview photograph of 942/677-59 trunk segment, with possible claw marks.

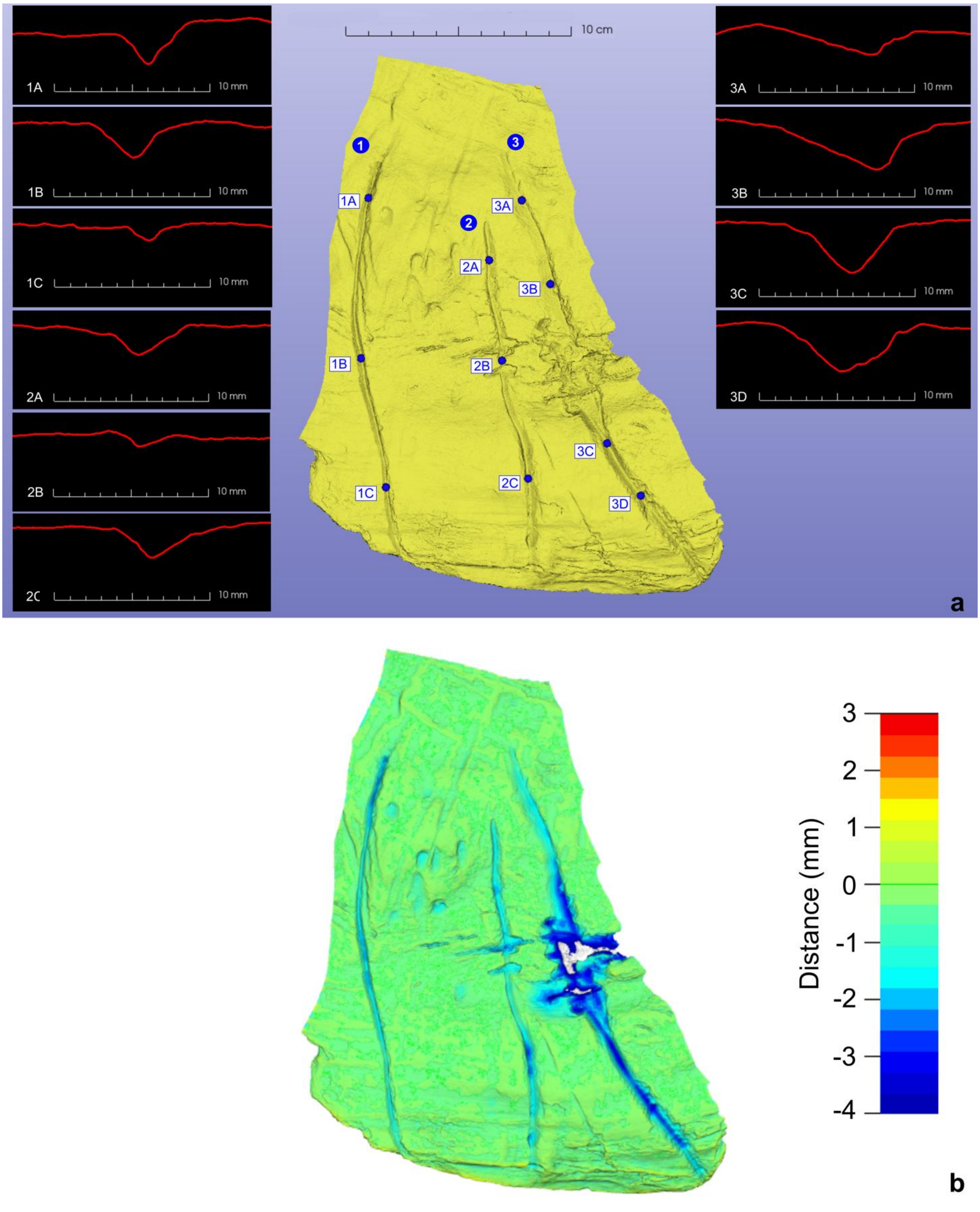

Figure S16: 3D representation of the 942/677-59 segment showing the location of the profiles and cross-sectional profiles (a), and the depths of the hypothesized claw marks.

3. 3D Models

3D Models and videos of the microCT scans of wood specimens are available to download open access on Zenodo: https://doi.org/10.5281/zenodo.17414562 (5).

4. Taxonomic identification of wood samples

The taxonomic identification of the wooden remains was undertaken at the M.H. Wiener Laboratory for Archaeological Science, American School of Classical Studies at Athens. Identification was based on observation of anatomical features on all three anatomy sections (tangential, radial and cross-section), where possible. However, the woody tissue was, with few exceptions, taphonomically compressed, and this condition severely affected the observation and characterization of anatomical features in the cross-section. The wood anatomy in the longitudinal sections (tangential and radial) was less affected by compression; therefore, microscopic observation concentrated mostly on these sections.

For the taxonomic identification of the specimens 940/673-39, 935/671-13 and 942/677- 59, the Leica DMLM microscope with X50 to X500 lenses was used for the observation of the wood anatomy. Additionally, small samples were extracted from each specimen with a razor blade and were mounted with water on a slide with a cover glass for observation under a transmitted light microscope. The sample was extracted from damaged parts of the specimens after the macro- and micro-morphological examination for signatures of human modification, always recording the exact sampling point. Wood anatomy literature (6, 7) and the reference collection of the Wiener Laboratory were used for the taxonomic identification.

For the micrographs (Figs. S3, S4, S9 and S10), we used the Leica DMLM microscope with Leica FLEXCAM C1 camera, and for the z-stacking, the software of Leica LAS X. Characteristic wood anatomy features of the studied specimens were compared with reference material (Figs. S3, S4, S9 and S10) from Schoch et al. (4). The comparative material is reproduced with permission from W. Schoch, who retains the copyright for these images.

The anatomical features that allowed for the identification of the taxa *Alnus* and *Salix/Populus* were observed in the longitudinal sections. In the case of specimen 935/671-13, although this roundwood piece was not compressed in its cross-section, it was not sampled transversally to avoid damage on the surfaces with signs of human modification. On the longitudinal section, the characteristic large and simple ray-vessel pits of the Salicaceae, smaller inter-vessel pits, and simple perforation plates in vessels were observed. The microCT scan image of the transverse section in Figure 4 indicates diffuse-porous distribution with small vessels that are in line with the *Salix/Populus* assignment of the specimen. Specimens 940/673-39 and 942/677-59 were both very compressed. The features on the longitudinal sections that pointed to their identification as *Alnus* sp. included uniseriate, homogeneous rays, small pits on vessel walls, and long scalariform perforations with >15 bars. The botanical identification of the three specimens agrees with the rest of the wood and wood charcoal assemblage from MAR 1, which is characterized by low taxonomic diversity and is dominated by *Alnus* and *Salix/Populus* with rare findings of other taxa (8).

5. Analysis of 942/677-59 ichnofossils

To acquire the surface cross-section profiles of the claw marks of specimen 942/677-59, we calculated a best-fit plane (least squares) (i.e., 9) using three points. These points were sampled approximately perpendicular to the longitudinal axis of the groove. The middle point was placed in the maximum curvature surface of the groove, and the other two were on both sides. While the plane represents the best fit, absolute perpendicularity to the axial plane is not calculated algebraically but using manual adjustments while observing the surface from an anterior point of view. After acquiring the contour that intersects the surface with the plane, we projected both on the coronal plane to present the XY plane without further angular distortions. We calculated ten of them for three claw marks of 942/677-59. We followed this workflow in the 3D Slicer platform (10) utilizing the Python extension in it. Measurements in the profiles were taken after Bello et al. (2) and Maté González et al. (3) with the use of ImageJ (11).

To provide a descriptive representation of the depths of the claw marks (3D topographic representation), we calculated a signed distance map (12), implemented in the Morpho::meshDist() function in R software (13). This algorithm applies a signed distance field on a surface mesh, indicating the distance from one surface to another. To do so, we have removed the claw marks and additional grooves on the surface of 942/677-59. In the next step, we decimated this surface to achieve an 80% reduction of its face number. Afterward, we filled these enclosed voids with an artificial triangulated grid, which was calculated by restricting the construction between the surrounding 942/677-59 vertices in Blender software (version 3.1.0; https://www.blender.org). This new mesh approximated the surface of 942/677-59 as if it had no grooves. Since the original surface is not plane but curved in many directions, the artificial surfaces may exceed height or appear below the original surface. We submitted this new surface mesh into Humphrey's Classes smoothing algorithm to enhance the relative topographic alternations. This algorithm is an optimized version of the Laplacian smoothing algorithm, abbreviated HC-Laplacian (14). The algorithm is implemented in R's Rvcg::vcgSmooth() function (13). We used 15 iterations. The distance map was calculated between this new smoothed surface and the original 942/677-59 surface. Depressions exceeding the 4mm threshold are depicted in white color. The tolerance threshold for an identical match between surfaces was set to 0.01 mm, represented by a green color.

6. Contemporary beaver activity on wood

Two types of beaver are known from Pleistocene contexts: the extant Eurasian beaver (*Castor fiber*), which is currently increasing in numbers across Eurasia, and the extinct giant beaver genus *Trogontherium*. While both species co-existed with and were exploited by Pleistocene *Homo* (e.g.15), only *Castor* has been identified at MAR-1 (16). To compare the wood remains from MAR-1 with wood modified by beavers, one of us (AM) visited Ham Fen nature reserve in August 2025. Ham Fen is a 41-hectare reserve managed by the Kent Wildlife Trust consisting of an ancient fenland. Beavers were legally reintroduced there in 2001, and their activity is now widespread, with wetlands having replaced a mixed-oak woodland over the past 24 years. Beavers consume a variety of wood types, with willow/poplar being a preferred food source (17), and this species is abundant at Ham Fen. Beavers also fell other tree species, particularly for construction purposes. For this study, wood was collected from dams and from the site of a felled willow tree to produce comparative images for analysis alongside the MAR-1 specimens.

The collected beaver-modified wood exhibits several characteristic features: bark stripping, chewed ends of branches and trunks, chewed-off branch attachments, shallow grooves across debarked surfaces, notches, and wood chips. Beavers partially or fully debark wood to consume the bark, either at the felling site or after transporting it to a food cache (17, 18). They gnaw through branches and small trunks to transport them to dams and dens, where the wood serves both as food and building material.

For the present study, we observed that ends of branches and/or trunks are gnawed into bevelled points with angles of approximately 30° to 35° to the branch/trunk axis (Fig. S13, e). Typically both ends of a branch are chewed this way, presumably to create transportable lengths. The surfaces of these beveled ends have clear tooth marks visible across the gnawed surface (Fig. S13, e and g). Tooth mark widths can vary depending on the age of the beaver (17, p.66), and on the wood samples collected from Ham Fen the tooth marks measure ca. 3-5 mm in width (Fig. S13, g). Shallow grooves are also visible across debarked and partially debarked branch surfaces, oriented approximately perpendicular to the direction of growth of the branch (Fig. S13, e and h). Wood chips can be found around the base of felled trees (Fig. S13, d and f). These also frequently have bevelled or rounded ends, exposing annual growth rings (Fig. S13, f). Stumps of trunks felled by beavers can be more circumferentially pointed than the smaller branches brought to dams and dens, with the chewed stump surface characterised by wide facets (Fig. S1, d). A further characteristic of beaver activity on wood includes notches that are perpendicular to growth, creating a so-called ‘melon slice’ (e.g. 17, p.184, 19, p.348); however examples of such gnawing were not seen on any of the material from Ham Fen.

The beveled points created by beaver gnawing are distinctive, and differ markedly from the shaped ends of the two wooden tools identified at MAR-1, ID 940/673-39 and ID 935/671-13 (see Figs. 2 and 3 in main manuscript). Unlike beavers, Pleistocene humans using stone tools typically worked with the grain of the wood, as evidenced by tool marks on other Pleistocene wooden artefacts (see also for comparison Figs. 14 and 15 in reference 20, and Figs. S3, and S8 in reference 1). Anthropogenic modification on other Pleistocene wooden tools can also include occasional sharp and thin marks running obliquely across a trunk or branch shaft attributed to debarking mistakes with the sharp edge of a stone flake (e.g. 20). On both of the MAR-1 specimens, tool marks either indicate working parallel to direction of growth (Fig. 2., a, b, d-f; Fig. 3, a) or, more rarely, obliquely to the grain (Fig. 3, b). In order to shape wooden tools, Pleistocene hominins do not appear to have cut across branches or trunks in the way that beavers do, but either rather worked along the surface with or against the grain of wood, or split the wood. As above, in contrast, beaver tooth marks overlying barked or debarked branch/trunk surfaces are perpendicular to the direction of growth, while tooth marks running across cut branch/trunk surfaces are regular, distinctive, and very visible.

Supplementary References

1. D. Leder, et al. The wooden artifacts from Schöningen's Spear Horizon and their place in human evolution. *Proc. Natl. Acad. Sci. U.S.A.* 121, e2320484121 (2024). https://doi.org/10.1073/pnas.2320484121.
2. S.M. Bello, I. De Groote, G. Delbarre. Application of 3-dimensional microscopy and micro-CT scanning to the analysis of Magdalenian portable art on bone and antler. *J. Archaeol. Sci.* 40, 2464–2476 (2013).
3. M.Á. Maté González, J. Yravedra, D. González-Aguilera, J.F. Palomeque-González, M. Domínguez-Rodrigo. Micro-photogrammetric characterization of cut marks on bones. *J. Archaeol. Sci.* 62, 128–142 (2015).
4. W. Schoch, I. Heller, F.H. Schweingruber, F. Kienast. Wood anatomy of central European Species (2004). Available online at: www.woodanatomy.ch.
5. A. Milks, et al. Evidence of the earliest hominin use of wooden hand-held tools found at Marathousa 1 (Greece) [Data set]. Zenodo. https://doi.org/10.5281/zenodo.17414561 (2025).
6. F.H. Schweingruber. *Anatomie Europäischer Hölzer*. Verlag, Bern und Stuttgart.
7. R. Gale, D. Cutler. *Plants in Archaeology: Identification Manual of Vegetative Plant Materials Used in Europe and the Southern Mediterranean to c. 1500* (Westbury, West Yorkshire and Royal Botanic Gardens, Kew, 2000).
8. M.H. Field, et al. A palaeoenvironmental reconstruction (based on palaeobotanical data and diatoms) of the Middle Pleistocene elephant (Palaeoloxodon antiquus) butchery site at Marathousa, Megalopolis, Greece. *Quat. Int.* 497, 108–122 (2018).
9. S. Benazzi, F.L. Bookstein, D.S. Strait, G.W. Weber. A new OH5 reconstruction with an assessment of its uncertainty. *J. Hum. Evol.* 61, 75–88 (2011).
10. A. Fedorov, et al. R. 3D Slicer as an image computing platform for the Quantitative Imaging Network. *Magn. Reson. Imaging* 30, 1323–1341 (2012).
11. M.D. Abràmoff, P.J. Magalhães, S.J. Ram. Image processing with ImageJ. *Biophotonics Int.* 11, 36–42 (2004).
12. J.A. Bærentzen, H. Aanæs. Generating signed distance fields from triangle meshes. *Informatics and Mathematical Modelling* (2002). http://www.imm.dtu.dk/pubdb/p.php?1833.
13. S. Schlager. Morpho and Rvcg – Shape analysis in R: R-packages for geometric morphometrics, shape analysis, and surface manipulations. In: G. Zheng, S. Li, G. Székely (Eds.), *Statistical Shape and Deformation Analysis*, pp. 217–256 (Academic Press, 2017).
14. J. Vollmer, R. Mencl, H. Mueller. Improved Laplacian smoothing of noisy surface meshes. *Comput. Graph. Forum* 18, 131–138 (1999).
15. S. Gaudzinski-Windheuser, L. Kindler, W. Roebroeks. Beaver exploitation, 400,000 years ago, testifies to prey choice diversity of Middle Pleistocene hominins. *Sci. Rep.* 13, 19766 (2023). https://doi.org/10.1038/s41598-023-46956-6.
16. G.E. Konidaris, et al. The Late Early–Middle Pleistocene Mammal Fauna from the Megalopolis Basin (Peloponnese, Greece) and Its Importance for Biostratigraphy and Paleoenvironment. *Quat.* 7, 41 (2024). https://doi.org/10.3390/quat7040041.
17. B. Coles. *Beavers in Britain's Past* (Oxbow Books, 2006).
18. M.J. Abbott, et al. Beaver-dredged canals and their spatial relationship to beaver-cut stumps. *Proc. Ind. Acad. Sci.* 121, 91–96 (2012).
19. M. Bamforth, M. Taylor, A. Little, A. Radini. Woodworking technology. In: N. Milner, C. Conneller, M. Taylor (Eds.), *Star Carr Volume 2: Studies in Technology, Subsistence and Environment*, pp. 347–366 (White Rose University Press, Heslington, 2018).
20. A. Milks, et al. A double-pointed wooden throwing stick from Schöningen, Germany: Results and new insights from a multianalytical study. *PLoS ONE* 18, e0287719 (2023). https://doi.org/10.1371/journal.pone.0287719.